Molecular Dynamics Simulation with the Charge Response Kernel: Vibrational Spectra of Liquid Water and *N*-Methylacetamide in Aqueous Solution

Satoru Iuchi, Akihiro Morita, and Shigeki Kato*

Department of Chemistry, Graduate School of Science, Kyoto University, Kitashirakawa, Sakyo-ku, Kyoto 606-8502, Japan

Received: October 10, 2001; In Final Form: January 28, 2002

New polarizable and flexible water models are developed using the charge response kernels obtained by ab initio calculations. MD simulations are carried out for three- and five-site models to compute the infrared (IR) and Raman spectra of liquid water at ambient conditions, and results are compared with those from other water models. On the basis of those calculations, we devised a new polarizable and flexible five-site model for the water molecule which can well reproduce the experimental spectral features. The model is also applied to computing the IR spectrum of *N*-methylacetamide in aqueous solution. The results imply the importance of the polarization effect for precise modeling of the intermolecular interaction.

1. Introduction

Dynamics of molecular processes in solution is one of the most important subjects of theoretical chemistry. The computer simulation has been quite powerful to elucidate a variety of experimental spectra and to reveal detailed dynamics at molecular level. For the computer simulations, proper intermolecular potential functions are crucial;[1−5] those should be simple so as to be implemented into feasible simulations and also accurate so as to reproduce the properties of actual liquids. Modeling of the intermolecular potential so far has mostly been based on the assumption of empirical pairwise potential where the intermolecular potential is expressed as the sum of site−site interactions, usually consisting of the short-range repulsion and the electrostatic interaction. This type of potential functions includes ST2,[6] TIP3P,[7] TIP4P,[8] TIP5P,[9] SPC,[10] and SPC/E[11] for water and AMBER,[2] CHARMM,[3] and OPLS[4] for various organic and biological molecules. Those pairwise functions have been widely successful to give a good description of liquid properties at a relatively modest cost of computations.

Despite the success of those empirical functions, other types of molecular models have been developed for more accurate simulations. Because one of the main shortcomings of those empirical pairwise potentials is in the lack of explicit polarization effects, several polarizable models have been proposed to include many-body polarization effects in the intermolecular functions. One of the simplest extensions of pairwise potentials is the point-polarizability model[12−22] where some of the sites carry polarizabilities besides the usual site−site pairwise parameters to incorporate the induced dipole moment as the response to electric field. This type of modeling is widely used in simulation studies to demonstrate that the explicit inclusion of many-body polarization effects could improve the description in various aspects, e.g., the diffusion coefficient of liquid water,[12−15] solvation structure around ion,[16−18] and solvation free energy.[19,20]

Recently, we have proposed the charge response kernel (CRK) model[23] as an alternative method to express the electronic polarization effect. Molecular dynamics (MD) calculations with the CRK have been performed for evaluating the anomalously slow diffusion of pyrazinyl radical in methanol solution[24] and for investigating fast vibrational relaxation of azide ion in water.[25] CRK is defined as $K_{ab} = \partial Q_a/\partial V_b$, where Q_a is the partial charge at the intramolecular site a and V_b is the electrostatic potential acting on the site b and describes the intramolecular charge redistribution induced by the external electrostatic potential in the site representation. Although the fluctuating charge (FQ) model proposed by Berne and co-workers[26,27] is derived from the similar concept of CRK model, the FQ model is based on the empirical formulation to represent the electron redistribution in a molecule and contains empirical parameters. On the contrary, the CRK is formulated on the basis of ab initio molecular orbital (MO) theory. Thus, the CRK as well as the partial charges are fully determined via ab initio MO calculations with no ambiguities, and no empirical optimization is necessary when the ab initio calculations are sufficiently accurate. Therefore, the CRK model enable us to explore the polarization effects in a variety of solutions on the same footing. The CRK can also fully describe the nonlocal charge redistribution through the off-diagonal elements, whereas the induced polarization is essentially local in the point-polarizability model. Such nonlocal response would be crucial especially to molecules which have delocalized π electrons.[23] Regardless of the above merits, the CRK is as easily and straightforwardly implemented in the actual simulations as both the point-polarizability and FQ models.

In the present paper, we develop new polarizable water models using the CRK approach. For the water modeling, a problem might occur to describe the out-of-plane induced polarization when the interaction sites were placed on the three atoms of a water molecule. This problem was avoided by introducing fictitious out-of-plane sites. The formulation and definition of the partial charges and CRKs are straightforward for those fictitious sites. The water models thus developed is applied to computing the infrared (IR) absorption and depolarized Raman scattering (DRS) of liquid water via MD simulations in order to verify the reliability of the models. We deal with IR and DRS because those spectra relevant to the intermolecular dynamics have been shown to be sensitive to the water model, especially to the induced electronic polarization effect.[28−34] Although the truncated adiabatic basis set (TAB) model[35,36] which explicitly treats with the polarization effect on the basis

10.1021/jp013773y CCC: $22.00
Published on Web 03/08/2002

of the electronic structures and the DFT based ab initio MD[37] have been recently applied to computing the IR and DRS spectra of liquid water, we show that the performance of the CRK model is almost equivalent to those models despite its simplicity. It is worthy noting that Stern et al. have very recently developed a new five-site water potential function based on the FQ and polarizable dipole models.[38]

We further apply the present water model to the *N*-methylacetamide (NMA)/water system. NMA is a model compound for the peptide unit, and thus, its solvation mechanism in water has been extensively studied.[19,27,39−42] The solvation effect on the vibrations of NMA has also been investigated both theoretically[43] and experimentally[44] because NMA can be regarded as one of the simplest models for understanding the protein secondary structure through vibrational spectroscopy. In hydrogen-bonded liquids such as water or alcohols, the effect of electronic polarization is crucial to the vibrational spectra.[28−34] Therefore, we focus on the polarization effect to interpret the IR spectra of NMA.

The remainder of this paper is as follows. In section 2, we present the details of the modeling for water and NMA molecules. In section 3, we describe the method to incorporate it into MD simulation and the results of the equilibrium properties are discussed. The results of calculations of IR and DRS spectra are presented in section 4 for bulk water and in section 5 for NMA in aqueous solution. The conclusions follow in section 6.

2. Molecular Modeling

2.1. Charge Polarization. The details of CRK model based on ab initio MO theory have been described elsewhere;[23,24] we only outline the method pertinent to the present calculations.

In the condensed phase, the solvent effects on a solute molecule are considered through the electrostatic potential originating from the surrounding solvent charges. Using the interaction site model, the Hamiltonian for the solute electronic state in solution may be written as

$$\hat{H} = \hat{H}_0 + \sum_a^{\text{site}} \hat{Q}_a V_a \tag{1}$$

where $\hat{H}_0$ is the gas-phase Hamiltonian, V_a is the electrostatic potential acting on the site a of a solute molecule, and $\hat{Q}_a$ is the effective charge operator at the site a.[23,45] Given the solute electronic wave function to be Ψ, the energy E and the partial charge Q_a are represented as

$$E = \langle \Psi | \hat{H} | \Psi \rangle \tag{2}$$

and

$$Q_a = \langle \Psi | \hat{Q}_a | \Psi \rangle \tag{3}$$

It is also easy to show that the partial charge Q_a is given as the derivative of the energy with respect to the electrostatic potential

$$Q_a = \frac{\partial E}{\partial V_a} \tag{4}$$

Thus, the CRK can be written as the second derivative of the total energy[23,24]

$$K_{ab} \equiv \frac{\partial Q_a}{\partial V_b} = \frac{\partial^2 E}{\partial V_a \partial V_b} \tag{5}$$

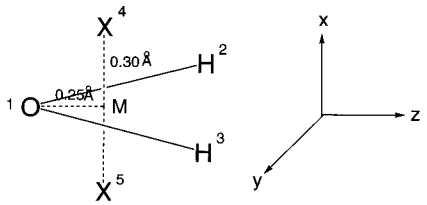

Figure 1. Geometry and site number of water. The interaction sites consist of "O", "H", "H", and two fictitious sites labeled "X". An auxiliary point "M" is introduced for defining X on the bisectional line of two OH bonds, where M−X is normal to the molecular plane.

In our previous work,[23] the CRK was calculated via coupled-perturbed Hartree−Fock (CPHF) equations for the restricted and unrestricted HF wave functions. We could derive the analytic expressions of Q_a and K_{ab} for the MP2 case, but here, we employ the numerical differentiations of the energy E with respect to the electrostatic potential V_a. The energy E under the electrostatic potential is calculated by the solvated Fock operator as described in ref 23.

The partial charges provide the dipole and quadrupole moments:

$$\mu_\alpha = \sum_a^{\text{site}} Q_a r_{\alpha a} \tag{6}$$

$$M_{\alpha\beta} = \frac{3}{2} \sum_a^{\text{site}} \left(r_{\alpha a} r_{\beta a} - \frac{r_a^{\,2}}{3} \delta_{\alpha\beta} \right) Q_a \tag{7}$$

and the CRKs give the polarizability:

$$\alpha_{\alpha\beta} = -\sum_{a,b}^{\text{site}} K_{ab} r_{\alpha a} r_{\beta b} \tag{8}$$

where $\alpha,\beta = x, y$, and z and $r_{\alpha a}$ denotes the coordinate of the site a. Those properties derived from Q_a and K_{ab} will be discussed and utilized in the later simulations.

2.2. Water. *Partial Charges and CRK.* The present model for a water molecule consists of five sites: three sites on the atoms and two out-of-plane sites, as shown in Figure 1. The two fictitious sites are necessary to describe the out-of-plane induced polarization. The locations of fictitious sites are not unique, and here, we followed Kim's TAB/10D model.[35] To see the effect of the out-of-plane polarization, the model consisting of only three sites on the atoms is also constructed.

The equilibrium geometry of a water molecule is taken from the experiment, $r_0 = 0.9572$ Å and $\theta_0 = 104.52°$,[46] whereas the partial charges and CRKs summarized in Table 1 are computed numerically by ab initio MP2/6-311G(2d,2p) calculations. The ab initio calculations should involve the electron correlation, because the HF calculations tend to yield substantially overestimated polarity. This overestimated polarity has in fact been utilized in the case of nonpolarizable models because it implicitly builds in the polarization effect in the condensed phase.[1] In the present model, however, the explicit polarization effect is included and the partial charges should reproduce the dipole moment of an isolated molecule, which is actually satisfied with the present level of calculations as seen in Table 2.

The dipole moment, quadrupole moment, and polarizability derived from eqs 6−8 are compared with the ab initio and experimental ones in Table 2. Note that the three-site model cannot reproduce the quadrupole moments and the out-of-plane

TABLE 1: Partial Charge Q_a and Charge Response Kernel K_{ab} of Water[a]

		Q_a	K_{ab}				
			(a) Three-Site Model				
1	O	−0.6970	−5.382	2.691	2.691		
2	H	0.3395		−2.342	−0.349		
3	H	0.3395			−2.342		
			(b) Five-Site Model				
1	O	−0.2700	−19.800	0.536	0.536	9.364	9.364
2	H	0.4800		−2.126	−0.132	0.861	0.861
3	H	0.4800			−2.126	0.861	0.861
4	X	−0.3450				−9.714	−1.372
						(−10.710)	(−0.376)
5	X	−0.3450					−9.714
							(−10.710)

[a] Values in the parentheses are for the modified five-site model. Unit: a.u.

TABLE 2: Dipole Moment μ, Polarizability α, Its Anisotropy $\Delta\alpha$, and Quadrupole Moment M of the Model CRK Water[a]

	three-site	five-site	ab initio	expt.	unit
μ	1.91	1.87	1.89	1.85[b]	Debye
α_{xx}	0.000	0.795 (0.984)	0.803	1.415[c]	Å^3
α_{yy}	1.208	1.209	1.220	1.528[c]	
α_{zz}	0.978	1.020	1.028	1.468[c]	
$\Delta\alpha$	1.111	0.359 (0.209)	0.361	0.098	Å^3
M_{xx}	−1.37	−2.18	−2.19	−2.50[d]	Buckingham
M_{yy}	1.44	2.22	2.30	2.63[d]	
M_{zz}	−0.07	−0.04	−0.11	−0.13[d]	

[a] The last two columns refer to ab initio and experimental values. Values in the parentheses are for the modified five-site model. [b] Reference 55. [c] Reference 65. [d] Reference 66.

component of the polarizability α_{xx} because of the lack of out-of-plane sites. The present ab initio calculations give generally smaller polarizabilities than the experimental values mainly because of the insufficient diffuse basis functions.[47] The reduced polarizabilities in solutions were predicted by an ab initio analysis,[48] because the spatially diffuse tail of the wave function is perturbed by the overlap with the neighboring molecules in the condensed phase.[24]

The polarizability anisotropy $\Delta\alpha$ is defined as

$$\Delta\alpha = \frac{1}{\sqrt{2}}[(\alpha_{xx} - \alpha_{yy})^2 + (\alpha_{yy} - \alpha_{zz})^2 + (\alpha_{zz} - \alpha_{xx})^2]^{1/2} \quad (9)$$

which is crucial to the Raman spectrum of liquid water.[28,36] Table 2 indicates significant overestimation of the polarization anisotropy $\Delta\alpha$ by the present five-site model over the experimental value. The large $\Delta\alpha$ is a consequence of the underestimated out-of-plane polarizability (α_{xx}) in our ab initio calculations, and therefore, we constructed a modified CRK by adjusting $K_{44}(=K_{55})$ and $K_{45}(=K_{54})$ so that α_{xx}/α_{zz} is consistent with the experiment. The modified CRKs and the resultant properties are also summarized with the parentheses in Tables 1 and 2. In this paper, we mainly focus on the modified five-site model and designate it simply as the five-site model. For comparison, we occasionally take up the results of the three-site and original five-site models.

Force Field. We discuss here the intramolecular potential of a water molecule. The anharmonicity of O−H stretching mode is important to reproduce the experimentally observed red-shift by a few hundred wavenumbers in the liquid phase.[49] Therefore, the Morse potential was introduced for the stretching mode, whereas the harmonic potential was used for the bending one.

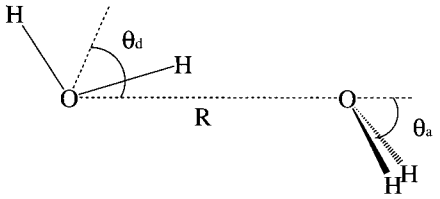

Figure 2. Water dimer geometry. Hydrogen bond length R, acceptor angle θ_a, and donor angle θ_d.

TABLE 3: Equilibrium Geometries and Binding Energies of Water Dimer[a]

	three-site	five-site	expt.[b]	unit
U	−4.01	−4.49	−5.40 ± 0.7	kcal/mol
R	2.97	2.98	2.98	Å
θ_a	15.2	49.9	57 ± 10	degree
θ_d	45.9	52.7	51 ± 10	

[a] The binding energy U, oxygen−oxygen distance R, acceptor angle θ_a, and donor angle θ_d. [b] Reference 67.

The internal vibrational potential is thus expressed as follows:

$$U_{\text{intra}} = D_{\text{OH}}[1 - \exp(-\rho\Delta r_1)]^2 + D_{\text{OH}}[1 - \exp(-\rho\Delta r_2)]^2 + f_r'\Delta r_1\Delta r_2 + \frac{1}{2}f_\theta r_0{}^2\Delta\theta^2 \quad (10)$$

where r_0 is the equilibrium bond length of water and Δr and $\Delta\theta$ are the displacements of the O−H bond length and the H−O−H angle from their equilibrium values. D_{OH} is the O−H dissociation energy experimentally determined to be 101.5 kcal/mol.[50] The harmonic force constants were determined by the least-squares fitting to the MP2/6-311G(2d,2p) energies as follows: f_r, f_r',, and f_θ are +8.717, −0.120, and +0.802 mdyn/Å, respectively. ρ is derived from the relation, $2\rho^2 D_{\text{OH}} = f_r$.

The intermolecular interaction was represented as the sum of site−site potential consisted of the Lennard-Jones (LJ) and Coulomb (CL) terms. The parameter ϵ_{OO} of the LJ potential was taken from the original SPC model[10] of 0.155 kcal/mol, whereas the van der Waals radii σ_{OO} was changed to 3.240 Å for avoiding the polarization catastrophe as discussed in section 3.1. This modification was introduced in another polarizable model.[12] The heterosite LJ parameters were determined by the standard combination rule.[51]

Water Dimer. To check the reliability of the present CRK models, a water dimer at the equilibrium configuration as illustrated in Figure 2 was examined in Table 3. In the three-site model, the binding energy U and the donor angle θ_a are significantly underestimated. The five-site model shows better performance in all of the items, though U is still underestimated from the experimental value. This is mainly attributed to the damping scale factor A in the short-range interactions, which will be discussed in section 3.1 in detail. Owing to the modified σ_{OO}, the present models well reproduce the experimental O−O distance.

2.3. NMA. *Force Field.* The partial charges and CRK of the NMA molecule were calculated at the same level of ab initio theory, MP2/6-311G(2d,2p). The interaction sites consist of all atoms including hydrogens, and the calculations of charges and CRK were carried out at the geometry optimized by the AMBER force field[2] with the partial charges in ref 52. The resultant optimized coordinates, partial charges, and CRK of NMA are provided in the Supporting Information. The dipole, quadrupole, and polarizability of NMA derived from eqs 6−8 and directly from the ab initio calculations are summarized in Table 4, where the agreement of the model with the ab initio values is

TABLE 4: Properties of NMA[a]

	model			ab initio			
	x	*y*	*z*	*x*	*y*	*z*	unit
μ	−2.944	−2.335	0.000	−2.937	−2.354	0.000	Debye
α	7.706	−0.399	0.000	7.812	−0.491	0.000	Å^3
		6.993	0.000		7.215	0.000	
			5.061			5.166	
M	1.199	−4.084	0.000	1.021	−4.029	0.000	Buckingham
		−0.026	0.000		0.005	0.000	
			−1.173			−1.026	

[a] See Figure 3 for the definition of the *xyz* axes.

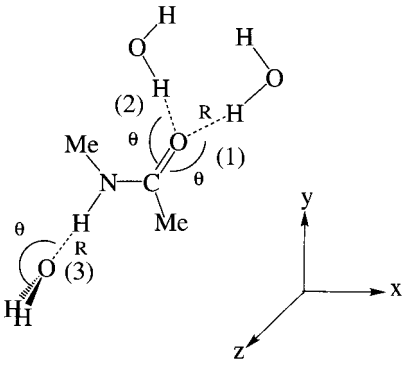

Figure 3. Molecular geometry of *N*-methylacetamide (NMA) in the *xyz* frame, where the *xy* plane is parallel to the molecular plane, and the *x* axis is parallel to the N−C bond. Three configurations 1, 2, and 3 are considered for NMA/water complex.

TABLE 5: Hydrogen Bond Lengths *R* (Å), Angles *θ* (deg), and Interaction Energies Δ*E* (kcal/mol) of NMA/Water Complexes[a]

	model			ab initio[b]		
	Δ*E*	*R*	*θ*	Δ*E*	*R*	*θ*
1	−5.9	1.95	131	−6.9(−7.8)[c]	1.98	115
2	−7.0	1.94	133	−7.3(−7.9)[c]	1.98	134
3	−5.1	2.04	180	−5.4(−5.5)[c]	2.12	177

[a] See Figure 3 for the definitions of the configurations (1), (2), and (3). [b] HF/6-31G* calculations taken from ref 42. [c] MP2/aug-cc-pVDZ calculations in ref 41.

satisfactory. The experimental dipole moment of an isolated NMA molecule was also well reproduced by the present model based on the MP2 calculation; $|\mu| = 3.7$ D for the experiment[21] and $|\mu| = 3.76$ D for the model.

We note that ab initio calculations of NMA at a fixed orientation of the methyl groups give different charges and CRKs among the three hydrogens of a methyl group, though they are equivalent under the internal methyl rotation. Therefore, during the MD simulations where the internal rotations are allowed, the averaged charges and CRKs were used for the equivalent hydrogen atoms in a methyl group.

The parameters for the intramolecular potential of NMA were taken from the AMBER[2] except for the partial charges Q_a^0 determined in the gas phase through the ab initio calculations described above.

NMA/Water Complex. To assess the performance of the present polarizable potential, the hydrogen bonded complexes of NMA with a water molecule were examined as illustrated in Figure 3. Because there is no experimental information on the NMA/water complex, we compare the present calculations with the previous ab initio ones used in simulation works.[27,42] Although the interaction energy for the configuration (1) is slightly underestimated as shown in Table 5, other values are very close to the target ones.

3. Molecular Dynamics Simulation

3.1. Simulation Procedure. *Formulation.* Because the details of MD simulations incorporating CRK were presented elsewhere,[24] we briefly outline the procedure. The total potential is expressed as follows:

$$U = \sum_{i>j}\sum_{a,b}^{\text{site}} u_{ai,bj}^{\text{LJ}}(|\boldsymbol{r}_{ai} - \boldsymbol{r}_{bj}|) + \sum_{i>j}\sum_{a,b}^{\text{site}} Q_{ai}Q_{bj}\frac{f(ai,bj)}{|\boldsymbol{r}_{ai} - \boldsymbol{r}_{bj}|} - \frac{1}{2}\sum_{i}\sum_{a,b}^{\text{site}} K_{ab}V_{ai}V_{bi} + \sum_i u_i^{\text{intra}} \quad (11)$$

where the suffixes *i* and *j* denote molecules and *a* and *b* the sites. $\boldsymbol{r}_{ai}$ is the coordinate of the site *a* of the *i*th molecule, and $u_{ai,bj}^{\text{LJ}}$ is the site−site Lennard-Jones potential. Q_{ai} and V_{ai} are the partial charge and electrostatic potential at the site *a* in the *i*th molecule. The first and second terms of eq 11 represent the LJ and CL interactions, respectively. The LJ interactions were cut off at the half of box size by using the tapering function.[24] The third term corresponds to the electronic reorganization energy because of the charge redistribution from the isolated condition. u_i^{intra} is the intramolecular vibrational potential.

The damping function $f(ai, bj)$ in eq 11 is introduced to attenuate the CL interactions in the short-range region and becomes unity at long range. The point charge model does not reasonably describe the CL interactions at a short distance where the electron clouds of two molecules overlap each other. This kind of attenuation is necessary in polarizable simulations; otherwise the partial charges would diverge during the simulations, so-called "polarization catastrophe". The form of damping function is given as[24]

$$f(ai,bj) = \begin{cases} \left(\frac{r}{s}\right)^4 - 2\left(\frac{r}{s}\right)^3 + 2\left(\frac{r}{s}\right) & \text{for } r < s \\ 1 & \text{for } r > s \end{cases} \quad (12)$$

where

$$s = A(\alpha_a\alpha_b)^{1/6} \quad (13)$$

Here α_a denotes the "volume" of the *a*th site derived from the atomic polarizability.[53] The volume parameters for the constituent atoms were determined as follows:[53] $\alpha_O = 0.862$ Å^3, $\alpha_H = 0.514$ Å^3, $\alpha_N = 1.105$ Å^3, and $\alpha_C = 1.405$ Å^3. The volume parameter of the fictitious site X in water was set to be $\alpha_X = 0.514$ Å^3 so as to reproduce the experimental heat of vaporization of water. *A* in eq 13 is a scaling factor of 2.6 as in ref 24, whereas the $A = 2.8$ was used for the flexible five-site model so as to reproduce the average dipole moment of liquid water.

The electrostatic potential V_{ai} is generated by the partial charges of the surrounding molecules and is thus given as

$$V_{ai} = \sum_{j(\neq i)}\sum_b Q_{bj}\frac{f(ai,bj)}{|\boldsymbol{r}_{ai} - \boldsymbol{r}_{bj}|} \quad (14)$$

whereas the charge Q_{ai} is the gas-phase charge Q_{ai}^0 plus the induced one via CRK:

$$Q_{ai} = Q_{ai}^0 + \sum_b^{\text{site}} K_{ab}V_{bi} \quad (15)$$

Equations 14 and 15 mean that V_{ai} and Q_{ai} are determined self-consistently. During the simulations, the tolerance for conver-

TABLE 6: Averaged Potential Energy $\bar{U}/N$, Solvation Coordination Number n, Dipole Moment $\bar{\mu}$, Diffusion Constant D, Optical Dielectric Constant ϵ_∞, and Static One ϵ_0 of Bulk Liquid Water[a]

	three-site	five-site	expt.	unit
$\bar{U}/N$	−7.76	−9.12	−9.92[b]	kcal/mol
n	5.52	5.49	5.2(0.4)[c]	molecule
$\bar{\mu}$	3.03(0.37)	2.90(0.30)	2.6[d]	Debye
D	2.2	1.6	2.3[e]	Fick
ϵ_∞	1.40	1.57	1.79[f]	
ϵ_0	379.2	86.6	78.5[f]	

[a] Values in parentheses are the standard deviations. [b] Reference 8. [c] Reference 54. [d] Theoretical estimate for ice in ref 68. [e] Reference 69. [f] Reference 58.

gence was $\Delta Q = 10^{-4}$ a.u. Typically, 5 to 10 iterations are necessary to achieve the convergence, and no energy drift was observed in the simulations. Because of the self-consistency between Q_a and V_a, no derivative of either Q_a or V_a is explicitly included in the force expression corresponding to the total potential U. In the actual simulation, however, the Ewald sum[51] was employed to correct the long-range interactions. The expressions of U and V_a are thus somewhat more complicated than eqs 11 and 14.

MD for Bulk Water and NMA/Water. MD simulations for the bulk water were performed with the periodic boundary conditions in the microcanonical (NVE) ensemble. The number of water molecules is 256 per cubic unit cell. The box length is $L = 19.73$ Å which corresponds to a density of 0.997 g/cm^3. The time propagation was performed by the Verlet algorithm[51] with the time step of 0.4 fs. Because the fictitious sites are massless, we cannot use the usual Newton equation of motion for them, and therefore, the constraint dynamics using the Lagrange multiplier was employed so that the two fictitious sites were always located at the same place; the crossing point M between the water plane and X−X line is assumed to always reside on the line bisecting the H−O−H angle, and the O−M and X−M distances are kept to be 0.25 and 0.30 Å as shown in Figure 1. The system was equilibrated at 25 °C with occasional temperature scaling for more than 40 ps, which was followed by the run of 100 ps with no temperature scaling.

To examine the effects of internal vibrations on the bulk water properties, we also carried out MD simulations with the molecular geometry fixed. The SHAKE algorithm[51] was used to fix the bond angles and lengths, and the time step was 2.0 fs.

MD simulation of the NMA/water system was performed with the same conditions except for the cubic unit cell containing one NMA and 253 water molecules. For a water molecule, we used the five-site model with the modified CRK.

3.2. Equilibrium Properties. *Bulk Water.* We examine some properties of the bulk water through the MD simulations to assess the reliability of the present models. The properties we treated here are the potential energy, coordination number (radial distribution function), dipole moment, diffusion constant, and dielectric constant which are summarized in Table 6.

The average potential energy per molecule, $\bar{U}/N$ in Table 6, well reproduced the value estimated by the experimental heat of vaporization[8] for the five-site model. The good agreement is a consequence of the parametrization of the scaling factor A and the volume parameter of the fictitious sites X, as discussed in section 3.1. For the three-site model, however, it is largely underestimated because of the lack of out-of-plane polarization. The coordination number n in the first solvation shell was determined by integrating the oxygen−oxygen radical distribution function $g_{OO}(r)$ up to the first minimum point at $r = 3.5$ Å. The calculated results are very close to the experimental value estimated by the neutron diffraction.[54] The peak positions and heights of $g_{OO}(r)$ and $g_{OH}(r)$ displayed in Figure 4 were also almost identical to those of previous models.[9,17,26,35,38]

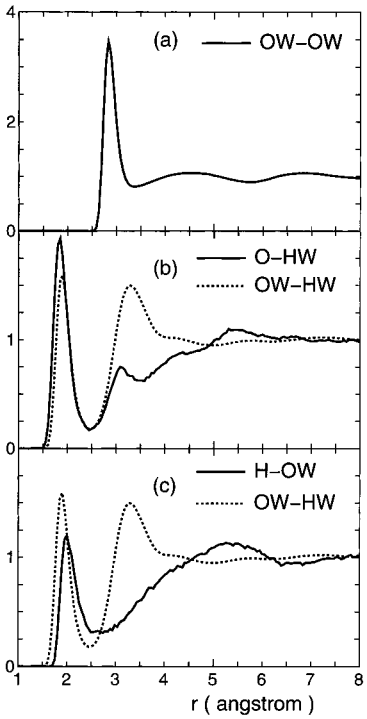

Figure 4. Radial distribution functions of (a) oxygen−oxygen of bulk water (g_{OW-OW}), (b) carbonyl oxygen−water hydrogen (g_{O-HW}), and (c) amide hydrogen−water oxygen (g_{H-OW}) of NMA/water mixture. In b and c, the oxygen−hydrogen function of bulk water (g_{OW-HW}) is also included for comparison (dotted line). The results of the five-site model are demonstrated for bulk water.

It is well-known that the average dipole moment of water molecules $\bar{\mu}$ is dramatically enhanced in the liquid over 1.85 D[55] in the gas phase as shown in Table 6. Although almost all of the dipole fluctuations are dominated by the component along the permanent dipole direction (z axis as in Figure 1), the fluctuations perpendicular to the z axis are not negligible; the standard deviations for the five-site model are 0.14 and 0.17 D for the x and y axes, respectively.

The diffusion constants D were calculated via the Einstein relation.[51] The CRK models gave improved values compared with the conventional rigid charge models where D is overestimated.

The dielectric constants can be evaluated by the linear response regime.[56] Although the five-site model has the optical dielectric constant ϵ_∞ in good agreement with the experiment, the three-site model gives a smaller value as a consequence of the lack of out-of-plane polarization. It is well-known that the static dielectric constant ϵ_0 converges very slowly, especially for polarizable models.[57] The 100 ps run of the three-site model gave the significantly overestimated value. Whereas the 250 ps run of the five-site model yielded $\epsilon_0 = 82.8$ close to 86.6 from the 100 ps run, it may not be converged yet. A longer time simulation might give much higher ϵ_0 considering that an averaged dipole moment exceeding 2.6 D leads to significant overestimation of ϵ_0 as discussed by Spirk.[57]

NMA/Water. The partial charges and dipole moment of NMA in aqueous solution are summarized in Table 7. The dipole moment is significantly enhanced in solution, and the partial

TABLE 7: Partial Charges and Dipole Moment μ of NMA in the Gas Phase and in Aqueous Solution[a]

atom	gas phase	aqueous	unit
N	−0.322	−0.365	a.u.
C	0.613	0.690	
O	−0.507	−0.701	
H	0.279	0.359	
CH_3(N)	0.052	0.095	
CH_3(C)	−0.115	−0.078	
μ	3.91	6.58	Debye

[a] For the methyl groups, the lumped partial charges of four atoms are given. CH_3(N) and CH_3(C) are the methyl group at the N and C site, respectively.

charges of the carbonyl oxygen (O) and amide hydrogen (H) are particularly enhanced because of the solute−solvent hydrogen bonding, consistent with previous simulation results.[27,42]

The hydrogen bond structure is apparent in the site−site radial distribution functions in Figure 4 between the carbonyl oxygen (O) and water hydrogen (HW) (g_{O-HW} in the upper panel) and between the amide hydrogen (H) and water oxygen (OW) (g_{H-OW} in the lower panel). Comparing these solute−solvent hydrogen bond structures with that of the bulk water given by g_{OW-HW}, the solute−solvent g_{O-HW} is somewhat higher in the first peak, implying a stronger hydrogen bond of O−HW than that of OW−HW. On the other hand, g_{H-OW} implies a weaker hydrogen bond than that in the bulk water for the same reason. Those insights are consistent with the previous studies[27,42] and also with the binding energies of the 1:1 NMA/water complex in two configurations as discussed in section 2.3. The stronger O−HW hydrogen bond than OW−HW one is attributed to a smaller van der Waals radius of O site than that of OW,[2] whereas the weaker H−OW bond than OW−HW to a smaller partial charge of the amide hydrogen site than the water hydrogen as shown in Table 7.

4. IR and Raman Spectra of Liquid Water

4.1. Methods. *IR Spectra*. Infrared absorption coefficient $\alpha(\omega)$ is computed from the autocorrelation function (ACF) of the total dipole moment of the system $\boldsymbol{M}(t)$:[59]

$$n(\omega)\alpha(\omega) = \frac{2\omega}{3\hbar cV\epsilon_{vac}} \tanh\left(\frac{\beta\hbar\omega}{2}\right) \int_0^\infty dt \cos(\omega t)\langle \boldsymbol{M}(t)\cdot\boldsymbol{M}(0)\rangle_{MD} \quad (16)$$

where $n(\omega)$ is the refractive index of the system at the frequency ω, c is the speed of light, V is the system volume, ϵ_{vac} is the vacuum permittivity, and $\beta = 1/k_BT$ with k_B and T being the Boltzmann constant and temperature, respectively. This expression includes the desymmetrization factor,[60] $2/(1 + e^{-\beta\hbar\omega})$, to satisfy the detailed balance condition, $I(-\omega) = \exp(-\beta\hbar\omega)\text{-}I(\omega)$.

To facilitate our understanding of the IR spectrum of liquid water, we define the partial correlation functions

$$C_M^{per}(t) = \sum_{i,j} \langle \boldsymbol{\mu}_i^{per}(t)\cdot\boldsymbol{\mu}_j^{per}(0)\rangle \quad (17)$$

$$C_M^{ind}(t) = \sum_{i,j} \langle \boldsymbol{\mu}_i^{ind}(t)\cdot\boldsymbol{\mu}_j^{ind}(0)\rangle \quad (18)$$

$$C_M^{cross}(t) = \sum_{i,j} (\langle \boldsymbol{\mu}_i^{ind}(t)\cdot\boldsymbol{\mu}_j^{per}(0)\rangle + \langle \boldsymbol{\mu}_i^{per}(t)\cdot\boldsymbol{\mu}_j^{ind}(0)\rangle) \quad (19)$$

where $\boldsymbol{\mu}_i^{per}$ and $\boldsymbol{\mu}_i^{ind}$ are the permanent and induced dipole moment of the ith water molecule.

We also considered two auxiliary spectra, i.e. the IR spectrum derived from the single molecule (1M) dipole correlation

$$[n(\omega)\alpha(\omega)]_{1M} = \frac{2\omega}{3\hbar cV\epsilon_{vac}} \tanh\left(\frac{\beta\hbar\omega}{2}\right) \int_0^\infty dt \cos(\omega t) \sum_i^{molecule} \langle \boldsymbol{\mu}_i(t)\cdot\boldsymbol{\mu}_i(0)\rangle \quad (20)$$

and the vibrational density of states (VDOS)

$$I_{VDOS}(\omega) = \frac{1}{\pi}\int_0^\infty dt \cos(\omega t) \sum_i^{molecule} \sum_a^{site} \langle \boldsymbol{v}_{ai}(t)\cdot\boldsymbol{v}_{ai}(0)\rangle \quad (21)$$

where $\boldsymbol{v}_{ai}$ is the velocity of the site a of the ith molecule. Equation 20 corresponds to the IR spectrum with eliminating the intermolecular cross correlation of the dipole motions, and therefore, the difference between eqs 16 and 20 would reveal how the intermolecular cross correlation affects the actual IR spectrum. Equation 21 will be utilized to straightforwardly characterize the nature of vibrations. For example, by restricting the summation over the site a in eq 21 to the water hydrogens, the result of VDOS spectrum would demonstrate the contribution of the hydrogen motion in a certain frequency region.

Raman Spectra. Raman scattering spectra are caused by the fluctuation of the total electronic polarizability.[61] In particular, the depolarized Raman scattering (DRS) arising from the polarizability anisotropy has been studied using various types of MD simulations.[28,31,36]

The total polarizability of the system is defined as the response of polarization $\boldsymbol{M}$ to the external field $\boldsymbol{e}$

$$\boldsymbol{\Pi} = \frac{\partial \boldsymbol{M}}{\partial \boldsymbol{e}}|_{\boldsymbol{e}=0} \quad (22)$$

$\boldsymbol{\Pi}(t)$ at the time t can be divided into two parts, a scalar (isotropic) component $\bar{\alpha}(t)\boldsymbol{I}$ and a second-rank (anisotropic) traceless component $\boldsymbol{\beta}(t)$:

$$\boldsymbol{\Pi}(t) = \bar{\alpha}(t)\boldsymbol{I} + \boldsymbol{\beta}(t) \quad (23)$$

where

$$\bar{\alpha}(t) = \frac{1}{3}\mathrm{Tr}\boldsymbol{\Pi}(t) \quad (24)$$

The reduced intensity of DRS is calculated by[31,59]

$$R(\omega) = \frac{2\omega}{(\omega_I - \omega)^4} \tanh\left(\frac{\beta\hbar\omega}{2}\right) \int_0^\infty dt \cos(\omega t)\,\langle \mathrm{Tr}(\boldsymbol{\beta}(t)\cdot\boldsymbol{\beta}(0))\rangle_{MD} \quad (25)$$

where ω_I is the frequency of the incident laser, 20 500 cm^{-1} (488 nm wavelength), and $\boldsymbol{\beta}$ is represented in the laboratory frame. This expression includes the desymmetrization to satisfy the detailed balance, $R(-\omega) = \exp(-\beta\hbar\omega)R(\omega)$ as in the case of IR spectrum. The Bose−Einstein corrected spectrum[28,31,36,62]

$$R^{BE}(\omega) = \frac{R(\omega)}{\omega} \quad (26)$$

will be employed instead of $R(\omega)$ itself to see the low-frequency region of the spectra.

The polarization anisotropy ACF in eq 25 is decomposed as follows. Because of the difference between the external field $\boldsymbol{e}$ in eq 22 and the local field acting on a constituent molecule,

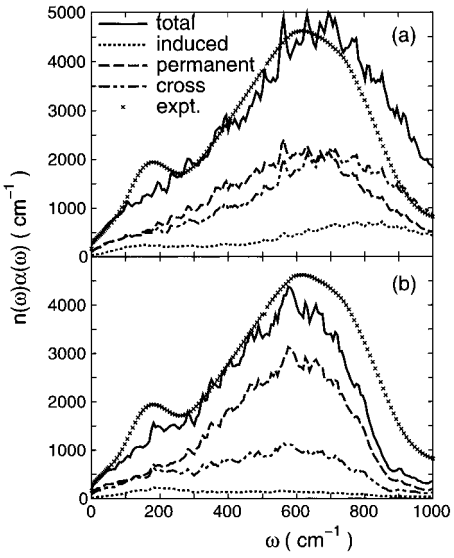

Figure 5. IR spectrum of liquid water in the low-frequency region. Total intensity (solid line) is decomposed into three components, induced (dotted), permanent (dashed line), and cross (two-dot dash line) terms. The experimental result in ref 63 is also shown (×) for comparison. (a) The three-site model. (b) The five-site model.

the total polarizability of the system $\mathbf{\Pi}$ is not equal to the sum of molecular polarizability and it is composed of two terms

$$\mathbf{\Pi} = \sum_i \boldsymbol{\alpha}_i + \mathbf{\Pi}^{\mathrm{ind}} \tag{27}$$

where $\boldsymbol{\alpha}_i$ is the molecular polarizability and $\mathbf{\Pi}^{\mathrm{ind}}$ is the induced one by the dielectric interaction. We calculated $\mathbf{\Pi}(t)$ by the three-point numerical differentiation of the total dipole moment $\boldsymbol{M}(t)$ with respect to weakly varying external field $\boldsymbol{e}$ for the instantaneous configuration at every recorded time step. The molecular polarizability $\boldsymbol{\alpha}_i(t)$ was simply determined by eq 8, and thus, the interaction induced part $\mathbf{\Pi}^{\mathrm{ind}}(t)$ was also available. To analyze the molecular and interaction induced polarizability, the polarization anisotropy $\boldsymbol{\beta}$ is decomposed as

$$\boldsymbol{\beta}(t) = \boldsymbol{\beta}^{\mathrm{mol}}(t) + \boldsymbol{\beta}^{\mathrm{ind}}(t) \tag{28}$$

The polarizability anisotropy ACF is then decomposed into three terms, i.e. the molecular, interaction induced, and their cross ones:

$$C_{\mathrm{DRS}}(t) = \langle \mathrm{Tr}(\boldsymbol{\beta}(t)\cdot\boldsymbol{\beta}(0))\rangle = C_{\mathrm{DRS}}^{\mathrm{mol}}(t) + C_{\mathrm{DRS}}^{\mathrm{ind}}(t) + C_{\mathrm{DRS}}^{\mathrm{cross}}(t) \tag{29}$$

where

$$C_{\mathrm{DRS}}^{\mathrm{mol}}(t) = \langle \mathrm{Tr}(\boldsymbol{\beta}^{\mathrm{mol}}(t)\cdot\boldsymbol{\beta}^{\mathrm{mol}}(0))\rangle \tag{30}$$

$$C_{\mathrm{DRS}}^{\mathrm{ind}}(t) = \langle \mathrm{Tr}(\boldsymbol{\beta}^{\mathrm{ind}}(t)\cdot\boldsymbol{\beta}^{\mathrm{ind}}(0))\rangle \tag{31}$$

$$C_{\mathrm{DRS}}^{\mathrm{cross}}(t) = \langle \mathrm{Tr}(\boldsymbol{\beta}^{\mathrm{ind}}(t)\cdot\boldsymbol{\beta}^{\mathrm{mol}}(0))\rangle + \langle \mathrm{Tr}(\boldsymbol{\beta}^{\mathrm{mol}}(t)\cdot\boldsymbol{\beta}^{\mathrm{ind}}(0))\rangle \tag{32}$$

4.2. IR Spectrum. We focus on the IR spectrum in the low-frequency region up to 1000 cm^{-1} because this frequency region reflects the intermolecular vibrations and is sensitive to the model of intermolecular potential. The previous experiments reported three IR bands in this frequency region around 60, 200, and 680 cm^{-1}.[50,63,64] The spectrum obtained from the five-site model is displayed in Figure 5 along with the one from the three-site model for comparison. The single molecule (1M) line shape function, eq 20, and the VDOS, eq 21, are shown in Figures 6 and 7.

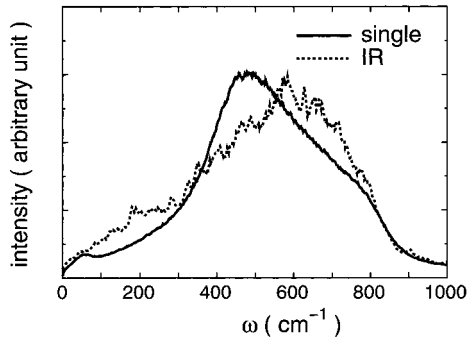

Figure 6. IR spectrum from single molecule line shape function (solid line). Full IR spectrum (dotted line) of the five-site model is included for comparison.

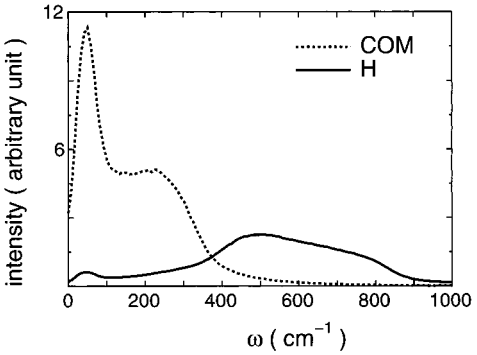

Figure 7. Vibrational density of states (VDOS) computed from the five-site model. The solid line is for hydrogen atoms and the dotted line for center of mass.

There is a broad peak around 600 cm^{-1} as shown in Figure 5. From the decomposition into the permanent and induced polarizations, the permanent part of ACF has a dominant contribution to this band, indicating that this band is attributed to water librational motion because the permanent dipole can vary only via the rotational motion.[36] Figure 6 indicates that the 1M line shape function qualitatively reproduces this main band, though its peak location is about 100 cm^{-1} lower in frequency. Also note that the 1M line shape is quite similar to the VDOS of hydrogen atoms in Figure 7, but not at all to the VDOS of the center of mass (COM) motion. All these results support the librational character of this main band. It is worth noting that the difference between the IR and 1M line shape function by about 100 cm^{-1} in frequency is attributed to the intermolecular cross correlation.

We mention here the performance of the three-site model to describe this band. Although the overall IR line shape of the three-site model appears fairly analogous to that of the five-site, the decomposition analysis of the three-site result reveals a relatively large contribution of the induced part to this band. This is because the lack of out-of-plane polarization in the three-site model overestimates the induced polarity associated with the librational motion. It suggests that the nonpolarizable three-site models proposed so far generally have this tendency, even though the polarization effects are implicitly included.[1]

The weak band at 200 cm^{-1} is discernible in the result of the five-site model. Figure 7 shows that there is no band in the VDOS of hydrogen atoms, but the VDOS of COM has a band in this region. It means that this band is related to the hindered translational motion, i.e., the hydrogen bonded O···O stretching.[36,37] The 1M line shape function in Figure 6 does not show

this 200 cm^{-1} band, indicating that the intermolecular correlation is quite important in this band. Actually, the decomposition analysis in Figure 5 shows that the induced part has a maximum in this frequency region.

Compared with the experiment,[63] the present calculations with the CRK models gave a weaker intensity of the 200 cm^{-1} band. The same tendency was also pointed out in the previous simulation studies.[28,32,33,36] Bursulaya et al. suggested that one of the potential sources of this tendency is the underestimation of the induced dipole moments.[36] In the present model, however, it is unlikely to the case because the averaged dipole moment in solution is slightly overestimated as shown in Table 6. They also implied that the intramolecular vibration could enhance this band.[36] However, we performed MD calculations with both the flexible and rigid molecular models and confirmed that the internal vibrations little affect the calculated IR spectra in this frequency region (figures are not shown here).

In the previous MD studies using polarizable models, the treatment of the polarization was often inconsistent; the explicit polarization effects were considered based on the trajectories obtained from the standard MD simulations with the nonpolarizable potential.[28−30,32−34] This means that the polarization influence on nuclear dynamics was ignored. Bosma et al.[28] and Guillot[33] suggested that the inclusion of the polarization effect in MD trajectories would be necessary to evaluate the induced dipole moments correctly. The present result does not support their suggestion because both the MD simulation and the subsequent analysis were performed using the same polarizable model in this work. We think eventually that the most plausible reason is the lack of explicit charge-transfer effect,[36] considering that ab initio MD yielded better intensity of this peak.[37]

Experiments[50,64] and theoretical work[36] suggested the existence of a very weak band around 60 cm^{-1} assigned to be the intermolecular O···O···O bending.[32,36,37] Although we did not confirm this band in our present IR results, it is clearly seen in the Raman spectra below.

4.3. DRS Spectrum. Figure 8 shows the calculated DRS spectra of liquid water up to 1000 cm^{-1}. In the experimental spectrum, three distinct bands at 60, 170, and 500 cm^{-1} are observed.[62] Here we compare the spectra calculated from the three water models, i.e. the 3-site, original and modified 5-site, with the experimental one.

The decomposition analysis discussed in section 4.1 was employed to characterize the three bands. Figure 8a indicates that the band at 500 cm^{-1} is dominated by the molecular part, whereas the band at 200 cm^{-1} is dominated by the interaction induced one. These results support the assignment that the former is attributed to the water librational motions, whereas the latter is attributed to the O···O stretching modes in the hydrogen bonded water molecules as in the IR spectrum. The band at 50 cm^{-1} is apparent in the DRS spectrum in Figure 8a. The decomposition analysis shows that both the molecular and induced part contribute to the 50 cm^{-1} band, and thus, both the rotational and translational motions are related with this band.

The original five-site model qualitatively show the same results as displayed in Figure 8b. The intensity around 500 cm^{-1} is, however, much greater than that around 200 cm^{-1}. This tendency is opposite to the experimental results.[62] This can be rationalized considering the emphasized polarizability anisotropy in the original five-site model as shown in Table 2. In fact, the result of the modified five-site model which has smaller polarizability anisotropy is consistent with the experiment. Because the three-site model is the most anisotropic, the librational character should be emphasized, which can be found in Figure 8c.

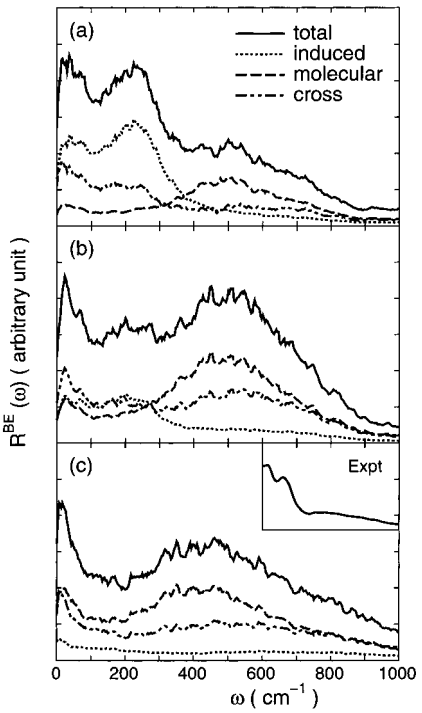

Figure 8. Depolarized Raman spectra of liquid water. (a) The (modified) five-site, (b) original five-site, and (c) three-site models. Dotted line is for induced, dash for molecular, and two-dot dash for cross terms. The experimental result in ref 62 is also shown in the inset of c.

The presence of both the 200 and 50 cm^{-1} band in the rigid five-site models (not shown here) indicates that the intramolecular vibration is not crucial to those bands, which corresponds with the results of the IR spectrum.

5. IR Spectrum of NMA in Aqueous Solution

The IR intensity of the NMA/water system is calculated by eq 16. Because the total dipole moment $\boldsymbol{M}(t)$ is composed of the solvents and solute contributions, the dipole ACF is decomposed into three parts

$$C_M(t) = C^{VV}(t) + C^{UU}(t) + C^{UV}(t) \tag{33}$$

where

$$C^{VV}(t) = \sum_{i,j}^{\text{solvents}} \langle \boldsymbol{\mu}_i(t)\cdot\boldsymbol{\mu}_j(0)\rangle \tag{34}$$

$$C^{UU}(t) = \langle \boldsymbol{\mu}_{NMA}(t)\cdot\boldsymbol{\mu}_{NMA}(0)\rangle \tag{35}$$

$$C^{UV}(t) = \sum_{i}^{\text{solvents}} (\langle \boldsymbol{\mu}_i(t)\cdot\boldsymbol{\mu}_{NMA}(0)\rangle + \langle \boldsymbol{\mu}_{NMA}(t)\cdot\boldsymbol{\mu}_i(0)\rangle) \tag{36}$$

Here $\boldsymbol{\mu}_i(t)$ is the dipole moment of the ith H_2O molecule and $\boldsymbol{\mu}_{NMA}(t)$ is that of NMA. The first term of eq 33 corresponds to the spectrum of solvent water and the second and third ones to that of NMA in water. Because many experimental works have discussed the spectrum obtained after subtracting the water spectrum,[44] we examined here the spectra computed from the latter two ACFs.

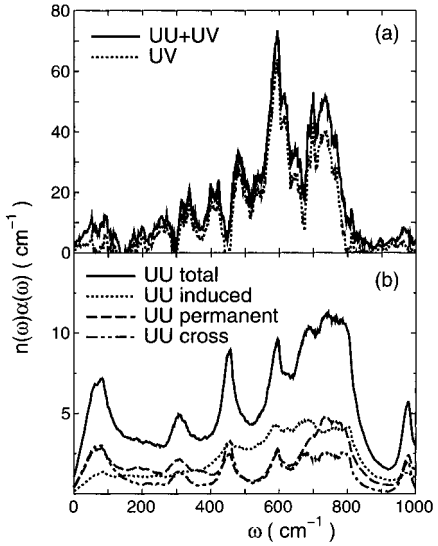

Figure 9. IR spectrum of *N*-methylacetamide in aqueous solution up to 1000 cm^{-1}. (a) Total IR spectrum with the UV term. (b) UU spectrum and its components.

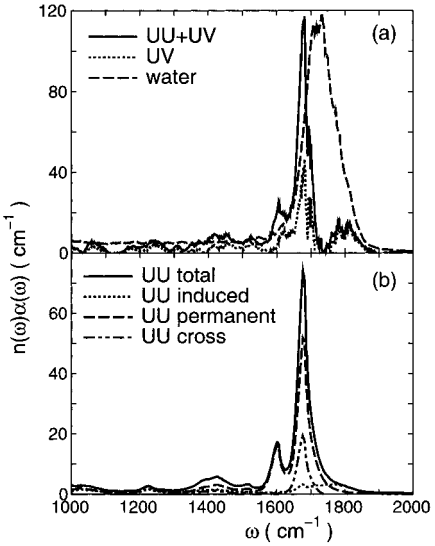

Figure 10. IR spectrum of *N*-methylacetamide in aqueous solution ranging from 1000 to 2000 cm^{-1}. (a) Total IR spectrum and UV term. Scaled IR spectrum of bulk water computed from the five-site model in section 4 is also included for comparison. (b) UU spectrum with its components.

The dipole moment of NMA is written as

$$\boldsymbol{\mu}_{\mathrm{NMA}}(t) = \boldsymbol{\mu}^{\mathrm{per}}_{\mathrm{NMA}}(t) + \boldsymbol{\mu}^{\mathrm{ind}}_{\mathrm{NMA}}(t) = \sum_{a}^{\mathrm{site}} Q^0_a \boldsymbol{r}_a(t) + \sum_{a}^{\mathrm{site}} [Q_a(t) - Q^0_a]\boldsymbol{r}_a(t) \quad (37)$$

where $\boldsymbol{\mu}^{\mathrm{per}}_{\mathrm{NMA}}$ and $\boldsymbol{\mu}^{\mathrm{ind}}_{\mathrm{NMA}}$ are the permanent and induced dipole moment of NMA and Q^0_a is the gas-phase charge, respectively. The first term of eq 37 is too crude to represent the gas-phase IR intensities because it neglects the change of partial charges because of the vibrations. We therefore replaced it by the ab initio one:

$$\boldsymbol{\mu}^{\mathrm{per}}_{\mathrm{NMA}}(t) = \boldsymbol{\mu}^{0}_{\mathrm{NMA}} + \sum_{a}^{\mathrm{site}} \sum_{\alpha=1}^{3} \frac{\partial \boldsymbol{\mu}}{\partial r_{\alpha a}} \Delta r_{\alpha a}(t) \; (\alpha = x, y, z) \quad (38)$$

where $\boldsymbol{\mu}^{0}_{\mathrm{NMA}}$ is the dipole moment at the equilibrium geometry and $\partial\boldsymbol{\mu}/r_{\alpha a}$ is the dipole derivative with $\Delta r_{\alpha a}$ being the displacement of the site *a*. All of the values were determined by MP2/6-311G(2d,2p) ab initio calculations at the optimized geometry using the present potential function. The IR intensity in the gas phase is given as $|\partial\boldsymbol{\mu}/\partial q_k|^2$ where q_k is the *k*th normal coordinate. The resultant Cartesian dipole derivative, normal vibrational frequencies, and IR intensities are provided in the Supporting Information.

C^{UU} in eq 35 is given as the sum of three terms, i.e., the permanent, induced, and cross terms as in the case of bulk water. We also decomposed the cross correlation function C^{UV} into four terms to facilitate the analyses of calculated spectrum.

Figure 9 displays the low-frequency spectral structure up to 1000 cm^{-1}. There are distinct bands at 720, 600, and 500 cm^{-1}. The band at 720 cm^{-1} is attributed to amide V mainly composed of the out-of-plane N−H bending. Because of the hydrogen bond, the permanent term at 720 cm^{-1} in the UU spectrum is broaden and blue shifted from the calculated gas-phase frequency of 688 cm^{-1}. Such a frequency shift by hydrogen bonding has been observed in the experiment.[44] The band at 600 cm^{-1} corresponds to amides IV and VI assigned to the in-plane NCO deformation and out-of-plane C═O bending, respectively. Because amide VI shows a blue-shift by the solvation from the calculated gas-phase frequency of 578 cm^{-1}, both amides IV and VI become very close in frequency in solution and become indistinguishable as shown in Figure 9. The band at 500 cm^{-1} is amide VII characterized by the in-plane NCO deformation. Although amide VII forms a sharp peak in the UU spectrum, it splits into two bands in the actual spectrum as seen in Figure 9a. Because the water librational motion appears at 500 cm^{-1} as shown in Figure 5, the splitting of amide VII is a consequence of the coupling between the water libration and NCO deformation.

Turning to the contributions of each component, the above-mentioned three bands are strongly enhanced by the induced term which are very broad in the region 400∼800 cm^{-1}. It is also apparent that the cross correlation (UV) term has large contributions to the spectrum; the magnitude of UV term is about 4 or 5 times that of the UU one. We found out that such an enhancement because of the UV term mainly comes from the cross term between the induced dipole of NMA and the permanent one of water.

The spectrum in the frequency region ranging from 1000 to 2000 cm^{-1} is shown in Figure 10. There are two distinct peaks at 1680 and 1600 cm^{-1}. These are assigned to amide I (C═O stretch) and amide II (in-plane N−H bend and C−N stretch). In contrast to the spectrum at the low-frequency region, the contributions from the permanent part are dominant in those bands. It may be a consequence of large dipole derivatives for those two modes; the IR intensities $|\partial\boldsymbol{\mu}/\partial q|^2$ are 8.85 and 3.53 D^2/Å^2 amu^{-1} for amides I and II, respectively. As is the case for the low-frequency structures, the intensities of these two peaks are enhanced by the UV term. The degree of enhancement is, however, smaller than that in the low-frequency region. As shown in Figure 10a, the water bending mode has a peak at the 1600∼1800 cm^{-1} region, and the coupling between the water bending and amide I occurs. As the result, the pronounced band at 1800 cm^{-1} appears mainly because of the UV term. Such a strong coupling of amide I with water bending has been suggested by the experiments.[44]

Although amide III is more discernible experimentally,[44] the intensity of the band at 1200 cm^{-1} is very weak in the present results, which comes from the underestimation of its dipole derivative in the gas phase: $|\partial\boldsymbol{\mu}/\partial q|^2 = 0.21$ D^2/Å^2 amu^{-1} for

amide III. In this respect, the refinement of the present NMA force field would be necessary in order to reproduce amide III band more accurately.

6. Concluding Remarks

In this study, we carried out MD simulation calculations for bulk water using new polarizable models with CRKs. The fluctuations of partial charge and polarizability were described by the CRK, and the polarization influence on nuclear dynamics was treated in a self-consistent manner. We constructed the three- and five-site models to see the importance of the out-of-plane polarization to the IR and DRS spectra. The effect of intramolecular vibrations on the spectral features are also examined.

To obtain a recommended CRK model to capture overall experimental features of the IR and DRS spectra, we proposed the modified CRK model whose polarizability anisotropy is relatively small and more consistent with the experimental value. This model could well reproduce the experimental spectral features including the relative intensity in the DRS spectrum.

We further applied the CRK model to computing the IR spectrum of NMA in aqueous solution. We found out that the induced polarization is very important to describe the local interactions such as hydrogen bonding between amide and water motions. The calculated IR spectra were consistent with the experimental findings except for the amide III band whose intensity is underestimated. We believe that the present results can be utilized to develop a more accurate NMA force field in aqueous solution. Considering that the AMBER force field gives small intensity for the amide III band in the gas phase, one of the possible ways to improve the agreement between the calculation and experiment would be to use the MP2 force field which is consistent with the dipole derivatives employed here.

Acknowledgment. This work was supported by the grant-in-aid from the Ministry of Education and Science, Japan. The MD simulations were carried out on the NEC SX-5 supercomputer at IMS computer center.

Supporting Information Available: Tables 1−5 showing optimized coordinates, partial charges, and CRK of NMA as well as the resultant Cartesian dipole derivative, normal vibrational frequencies, and IR intensities. This information is available free of charge via the Internet at http://pubs.acs.org.

References and Notes

(1) Kollman, P. A. *Acc. Chem. Res.* **1996**, *29*, 461.
(2) Cornell, W. D.; Cieplak, P.; Bayly, C. I.; Gould, I. R.; Merz, K. M., Jr.; Ferguson, D. M.; Spellmeyer, D. C.; Fox, T.; Caldwell, J. W.; Kollman, P. A. *J. Am. Chem. Soc.* **1995**, *117*, 5179.
(3) MacKerell, A. D., Jr.; Bashford, D.; Bellott, M.; Dunbrack, R. L., Jr.; Evanseck, J. D.; Field, M. J.; Fischer, S.; Gao, J.; Guo, H.; Ha, S.; Joseph-McCarthy, D.; Kuchnir, L.; Kuczera, K.; Lau, F. T. K.; Mattos, C.; Michnick, S.; Ngo, T.; Nguyen, D. T.; Prodhom, B.; Reiher, W. E., III.; Roux, B.; Schlenkrich, M.; Smith, J. C.; Stote, R.; Straub, J.; Watanabe, M.; Wiorkiewicz-Kuczera, J.; Yin, D.; Karplus, M. *J. Phys. Chem. B* **1998**, *102*, 3586.
(4) Jorgensen, W. L.; Tirado-Rives, J. *J. Am. Chem. Soc.* **1988**, *110*, 1657.
(5) Jorgensen, W. L. *Acc. Chem. Res.* **1989**, *22*, 184.
(6) Stillinger, F. H.; Rahman, A. *J. Chem. Phys.* **1974**, *60*, 1545.
(7) Jorgensen, W. L. *J. Chem. Phys.* **1982**, *77*, 4156.
(8) Jorgensen, W. L.; Chandrasekhar, J.; Madura, J. D.; Impey, R. W.; Klein, M. L. *J. Chem. Phys.* **1983**, *79*, 926.
(9) Mahoney, M. W.; Jorgensen, W. L. *J. Chem. Phys.* **2000**, *112*, 8910.
(10) Berendsen, H. J. C.; Postma, J. P. M.; van Gunsteren, W. F.; Hermans, J. In *Intermolecular Forces*; Pullman, B., Ed.; D. Reidel Publishing Co.: Dordrecht, The Netherlands, 1981; pp 331−342.
(11) Berendsen, H. J. C.; Grigera, J. R.; Straatsma, T. P. *J. Phys. Chem.* **1987**, *91*, 6269.
(12) Ahlström, P.; Wallqvist, A.; Engström, S.; Jönsson, B. *Mol. Phys.* **1989**, *68*, 563.
(13) Bernardo, D. N.; Ding, Y.; Krogh-Jespersen, K.; Levy, R. M. *J. Phys. Chem.* **1994**, *98*, 4180.
(14) Niesar, U.; Corongiu, G.; Clementi, E.; Kneller, G. R.; Bhattacharya, D. K. *J. Phys. Chem.* **1990**, *94*, 7949.
(15) van Belle, D.; Froeyen, M.; Lippens, G.; Wodak, S. J. *Mol. Phys.* **1992**, *77*, 239.
(16) Rullmann, J. A. C.; van Duijnen, P. T. *Mol. Phys.* **1988**, *63*, 451.
(17) (a) Sprik, M.; Klein, M. L.; Watanabe, K. *J. Phys. Chem.* **1990**, *94*, 6483. (b) Sprik, M. *J. Phys. Chem.* **1991**, *95*, 2283.
(18) (a) Dang, L. X.; Rice, J. E.; Caldwell, J.; Kollman, P. A. *J. Am. Chem. Soc.* **1991**, *113*, 2481. (b) Caldwell, J.; Dang, L. X.; Kollman, P. A. *J. Am. Chem. Soc.* **1990**, *112*, 9144.
(19) Ding, Y.; Bernardo, D. N.; Krogh-Jespersen, K.; Levy, R. M. *J. Phys. Chem.* **1995**, *99*, 11575.
(20) (a) Meng, E. C.; Cieplak, P.; Caldwell, J. W.; Kollman, P. A. *J. Am. Chem. Soc.* **1994**, *116*, 12061. (b) Sun, Y.; Caldwell, J. W.; Kollman, P. A. *J. Phys. Chem.* **1995**, *99*, 10081. (c) Meng, E. C.; Caldwell, J. W.; Kollman, P. A. *J. Phys. Chem.* **1996**, *100*, 2367.
(21) Caldwell, J. W.; Kollman, P. A. *J. Phys. Chem.* **1995**, *99*, 6208.
(22) Gao, J.; Pavelites, J. J.; Habibollazadeh, D. *J. Phys. Chem.* **1996**, *100*, 2689.
(23) Morita, A.; Kato, S. *J. Am. Chem. Soc.* **1997**, *119*, 4021.
(24) Morita, A.; Kato, S. *J. Chem. Phys.* **1998**, *108*, 6809.
(25) Morita, A.; Kato, S. *J. Chem. Phys.* **1998**, *109*, 5511.
(26) Rick, S. W.; Stuart, S. J.; Berne, B. J. *J. Chem. Phys.* **1994**, *101*, 6141.
(27) Rick, S. W.; Berne, B. J. *J. Am. Chem. Soc.* **1996**, *118*, 672.
(28) Bosma, W. B.; Fried, L. E.; Mukamel, S. *J. Chem. Phys.* **1993**, *98*, 4413.
(29) Madden, P. A.; Impey, R. W. *Chem. Phys. Lett.* **1986**, *123*, 502.
(30) Souaille, M.; Smith, J. C. *Mol. Phys.* **1996**, *87*, 1333.
(31) Saito, S.; Ohmine, I. *J. Chem. Phys.* **1995**, *102*, 3566.
(32) Saito, S.; Ohmine, I. *J. Chem. Phys.* **1994**, *101*, 6063.
(33) Guillot, B. *J. Chem. Phys.* **1991**, *95*, 1543.
(34) Ahlborn, H.; Ji, X.; Space, B.; Moore, P. B. *J. Chem. Phys.* **1999**, *111*, 10622.
(35) (a) Bursulaya, B. D.; Kim, H. J. *J. Chem. Phys.* **1998**, *108*, 3277. (b) Bursulaya, B. D.; Jeon, J.; Zichi, D. A.; Kim, H. J. *J. Chem. Phys.* **1998**, *108*, 3286.
(36) Bursulaya, B. D.; Kim, H. J. *J. Chem. Phys.* **1998**, *109*, 4911.
(37) Silvestrelli, P. L.; Bernasconi, M.; Parrinello, M. *Chem. Phys. Lett.* **1997**, *277*, 478.
(38) Stern, H. A.; Rittner, F.; Berne, B. J.; Friesner, R. A. *J. Chem. Phys.* **2001**, *115*, 2237.
(39) Guo, H.; Karplus, M. *J. Phys. Chem.* **1992**, *96*, 7273.
(40) Han, W.-G.; Suhai, S. *J. Phys. Chem.* **1996**, *100*, 3942.
(41) Dixon, D. A.; Dobbs, K. D.; Valentini, J. J. *J. Phys. Chem.* **1994**, *98*, 13435.
(42) Gao, J.; Freindorf, M. *J. Phys. Chem. A* **1997**, *101*, 3182.
(43) (a) Mirkin, N. G.; Krimm, S. *J. Am. Chem. Soc.* **1991**, *113*, 9742. (b) Mirkin, N. G.; Krimm, S. *J. Mol. Struct.* **1996**, *377*, 219. (c) Torii, H.; Tatsumi, T.; Tasumi, M. *J. Raman Spectrosc.* **1998**, *29*, 537.
(44) (a) Chen, X. G.; Schweitzer-Stenner, R.; Asher, S. A.; Mirkin, N. G.; Krimm, S. *J. Phys. Chem.* **1995**, *99*, 3074. (b) Chen, X. G.; Schweitzer-Stenner, R.; Krimm, S.; Mirkin, N. G.; Asher, S. A. *J. Am. Chem. Soc.* **1994**, *116*, 11141. (c) Song, S.; Asher, S. A.; Krimm, S.; Bandekar, J. *J. Am. Chem. Soc.* **1988**, *110*, 8547.
(45) Ten-no, S.; Hirata, F.; Kato, S. *J. Chem. Phys.* **1994**, *100*, 7443.
(46) Benedict, W. S.; Gailar, N.; Plyler, E. K. *J. Chem. Phys.* **1956**, *24*, 1139.
(47) Woon, D. E.; Dunning, T. H., Jr. *J. Chem. Phys.* **1994**, *100*, 2975.
(48) Morita, A.; Kato, S. *J. Chem. Phys.* **1999**, *110*, 11987.
(49) Toukan, K.; Rahman, A. *Phys. Rev. B* **1985**, *31*, 2643.
(50) Eisenberg, D.; Kauzmann, W. *The Structure and Properties of Water*; Oxford University: London, 1969.
(51) Allen, M. P.; Tildesley, D. J. *Computer Simulation of Liquids*; Oxford University Press: New York, 1991.
(52) Cieplak, P.; Kollman, P. *J. Comput. Chem.* **1991**, *12*, 1232.
(53) Thole, B. T. *Chem. Phys.* **1981**, *59*, 341.
(54) Soper, A. K. *J. Chem. Phys.* **1994**, *101*, 6888.
(55) Clough, S. A.; Beers, Y.; Klein, G. P.; Rothman, L. S. *J. Chem. Phys.* **1973**, *59*, 2254.
(56) Neumann, M.; Steinhauser, O. *Chem. Phys. Lett.* **1984**, *106*, 563.
(57) Sprik, M. *J. Chem. Phys.* **1991**, *95*, 6762.
(58) Buckingham, A. D. *Proc. R. Soc. London, Ser. A* **1956**, *238*, 235.
(59) McQuarrie, D. A. *Statistical Mechanics*; Harper Collins Publishers: New York, 1976.
(60) Borysow, J.; Moraldi, M.; Frommhold, L. *Mol. Phys.* **1985**, *56*, 913.

(61) Berne, B. J.; Pecora, R. *Dynamic Light Scattering*; Dover: New York, 2000.
(62) Walrafen, G. E.; Hokmabadi, M. S.; Yang, W.-H. *J. Chem. Phys.* **1988**, *88*, 4555.
(63) Bertie, J. E.; Lan, Z. *Appl. Spectrosc.* **1996**, *50*, 1047.
(64) Hasted, J. B.; Husain, S. K.; Frescura, F. A. M.; Birch, J. R. *Chem. Phys. Lett.* **1985**, *118*, 622.
(65) Murphy, W. F. *J. Chem. Phys.* **1977**, *67*, 5877.
(66) Verhoeven, J.; Dymanus, A. *J. Chem. Phys.* **1970**, *52*, 3222.
(67) Odutola, J. A.; Dyke, T. R. *J. Chem. Phys.* **1980**, *72*, 5062.
(68) Coulson, C. A.; Eisenberg, D. *Proc. R. Soc. London, Ser. A* **1966**, *291*, 445.
(69) Mills, R. *J. Phys. Chem.* **1973**, *77*, 685.